AGU PUBLICATIONS

Space Weather

RESEARCH ARTICLE
10.1002/2014SW001135

Key Points:
- Finite element modeling
- Transmission network coefficients
- Magnetic field data interpolation

Supporting Information:
- Text S1
- Table S1

Correspondence to:
E. Matandirotya,
electdom@gmail.com

Citation:
Matandirotya, E., P. J. Cilliers, and R. R. Van Zyl (2015), Modeling geomagnetically induced currents in the South African power transmission network using the finite element method, *Space Weather*, *13*, 185–195, doi:10.1002/2014SW001135.

Received 20 OCT 2014
Accepted 27 FEB 2015
Accepted article online 4 MAR 2015
Published online 24 MAR 2015

Modeling geomagnetically induced currents in the South African power transmission network using the finite element method

Electdom Matandirotya[1,2], Pierre J. Cilliers[1,2], and Robert R. Van Zyl[1]

[1] French South African Institute of Technology, Department of Electrical, Electronic and Computer Engineering, Cape Peninsula University of Technology, Cape Town, South Africa, [2] South African National Space Agency, Space Science Directorate, Hermanus, South Africa

Abstract Geomagnetically induced currents (GIC) are a result of time variations of the geomagnetic field, which induce a geoelectric field at the Earth's surface. Geomagnetic perturbations are enhanced during adverse space weather events called geomagnetic storms. All ground-based conductor networks can be affected by GIC during such events. As a way of assessing the magnitude of GIC expected in a particular technological system, models are developed, in which the computation of the induced geoelectric field is a key step. Computation of GIC in the South African power transmission network has so far been done using a uniform Earth model and improved using a layered Earth conductivity profile. In this work we present geoelectric field results obtained by using the finite element method (FEM) and improved GIC estimates using a realistic conductivity profile, magnetic field data interpolated from two South African observatories, and a new method for estimating the network coefficients, *a* and *b*, which map the north-south and east-west electric fields to their respective GIC components. The performance of the chosen FEM model demonstrates that it is an effective tool for GIC modeling. Unlike previous engineering techniques, our method for estimating the *a* and *b* coefficients from GIC and measured magnetic field data gives results that are independent of prior knowledge of the network configuration. The GIC estimated using the *a* and *b* coefficients obtained from the proposed method compares well with the measured GIC during the late October 2003 geomagnetic storm.

1. Introduction

Geomagnetically induced currents (GIC) resulting from space weather events are induced in various technical networks during temporal variations of the geomagnetic field as governed by Faraday's law of induction [e.g., *Paul*, 2004]. The interference of GIC with the technological systems is enhanced during adverse space weather events called geomagnetic storms. During a geomagnetic storm, the geomagnetic field experiences rapid temporal variations. These perturbations follow from a sudden increase in the energy transferred from the Sun to the magnetosphere and ionosphere. The energy transfer can initiate destabilization in the magnetosphere, thus causing geomagnetic storms [*Moldwin*, 2008].

The effects of space weather on power systems, oil, and gas pipelines have so far drawn much attention of the science and engineering communities, as the damage caused by the interference of GIC are costly [*Molinski*, 2002; *Bolduc*, 2002; *Kappenman*, 2007]. The ionospheric currents and Earth's conductivity profile both contribute to the characteristics of the induced geoelectric field which is the driver of GIC [*Boteler et al.*, 1998].

Two steps are required when GIC are computed in any technological system, namely, the geophysical step and the engineering step. The geophysical step is aimed at determining the induced horizontal geoelectric field. This step basically involves solving Maxwell's equations with appropriate electromagnetic boundary conditions. It has successfully been demonstrated that techniques such as the Complex Image Method [*Boteler and Pirjola*, 1998; *Pirjola*, 2002], the method of auxiliary sources [*Shepherd and Shubitidze*, 2003], and the spherical elementary current systems (SECS) [*Amm and Viljanen*, 1999] can be used efficiently in computing the geomagnetic fields and geoelectric fields associated with GIC.

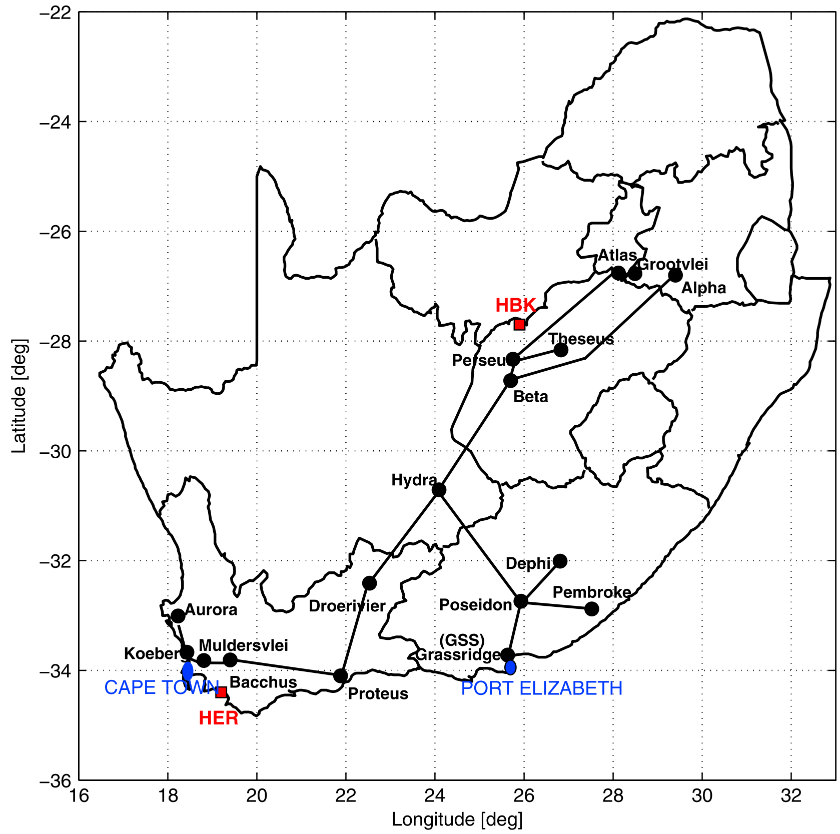

Figure 1. Map showing some of the South African 400 kV substations links and the locations of the geomagnetic observatories Hermanus (HER) and Hartebeesthoek (HBK) and the Grassridge (GSS) substation where the GIC recordings were done. HER is 670 km and HBK 1470 km away from GSS.

When dealing with a power network, the engineering step requires an accurate determination of the network coefficients *a* and *b*, in units of A km/V. These are network attributes that are unique to each network substation as they are dependent on the network configuration, i.e., the locations of the substations, transformer connections, lengths and resistances of the transmission lines, number of transformers at the substations, transformer winding resistances, and substation grounding resistances [*Wik et al.*, 2008]. For accurate modeling of GIC the network coefficients at the time of interest are necessary. The network coefficients may change with time through adding a transformer, inserting or removing a blocking capacitor or reconfiguring the transmission lines, or simply using a switch for a connection or disconnection of an equipment or a line.

2. GIC Modeling in the South African Network

After the evidence of GIC in the South African network was reported by *Koen* [2000], models have been developed to assess the vulnerability of the South African grid to GIC. Figure 1 shows the locations of two magnetic observatories Hermanus (HER) and Hartebeesthoek (HBK), which are within South Africa, part of the South African 400 kV network, and the substation Grassridge (GSS) where GIC were measured. *Koen* [2002] and *Bernhardi et al.* [2008a] discuss the performance of a uniform Earth model. *Bernhardi et al.* [2008a] used the SECS method for interpolating the magnetic field using data from three South African magnetic observatories, namely, HER, HBK, and Tsumeb (TSU). The model was improved by using a layered Earth conductivity profile and recomputing the network coefficients [*Ngwira et al.*, 2008]. In the previous work, two sets of network coefficients were used for Grassridge, namely, $a = -80$; $b = 15$ A km/V [*Bernhardi et al.*, 2008a] and $a = -80$; $b = 1$ A km/V [*Ngwira et al.*, 2008].

The FEM is introduced to handle geometric complexities in GIC modeling and to provide a means of finding the spatial distribution of the current density in the Earth. The FEM approximates solutions of a real complex problem using an idealized model. The technique divides the complex geometry into nonoverlapping but joined subdivisions referred to as elements. Element solutions are integrated to give the overall solution.

The application of FEM in the computation of the geoelectric field in connection with GIC modeling is a relatively new technique. The work reported by *Dong et al.* [2013] pioneered the application of FEM in GIC modeling. Compared to the modeling made by *Dong et al.* [2013], who used only simulated magnetic fields. The present work provides an extension of the application of FEM. The use of FEM enhances the understanding of how the induced electric field varies within the layers of the Earth. This study uses FEM for the first time to compute the induced geoelectric field using measured magnetic field data and a realistic layered ground conductivity profile as inputs. The geoelectric field obtained with FEM is used to derive GIC results which are compared with measured GIC.

In the present work, the finite element method (FEM) software, COMSOL Multiphysics [*COMSOL Inc.* 2014] is used to compute the electric field induced in a layered Earth in two cases. Case 1 uses magnetic field data measured at HER, and case 2 uses interpolated data from HER and HBK. The geomagnetic data from Tsumeb were not used in the current study as it is located too far from GSS for its magnetic field to have a significant effect on GIC at Grassridge [*Ngwira et al.*, 2009]. The interpolated data are an estimate of the magnetic field measured at Grassridge. The E_x and E_y computed from the interpolated data are assumed to be the local geoelectric field components at Grassridge.

3. Theory

The accurate determination of the geoelectric field that drives the GIC is a critical geophysical step in GIC modeling. The geoelectric field on and beneath the surface of the ground can be computed from the local measured geomagnetic field or from an interpolated geomagnetic field using an equivalent ionospheric current system. We adopt a Cartesian coordinate system where the *xy* plane corresponds to the Earth's surface and the *x* axis points northward, the *y* axis eastward, and the *z* axis downward. The Earth curvature is neglected in all computations. This is a reasonable approximation for distances less than 1000 km [*Pulkkinen*, 2003].

3.1. Calculating the Geoelectric Field From the Magnetic Field

The geoelectric field (**E**) and the geomagnetic field (**B**) are related to each other according to Faraday's law of induction (equation (1)) and Ampère's law (equation (2))

$$\nabla \times \mathbf{E} = \frac{\partial \mathbf{B}}{\partial t}, \tag{1}$$

$$\nabla \times \mathbf{B} = \mu_0 \left(\mathbf{J} + \epsilon \frac{\partial \mathbf{E}}{\partial t} \right), \tag{2}$$

where **J** is the current density in A/m^2, μ_0 is the magnetic permeability of vacuum in H/m, ϵ is the permittivity of the medium in F/m, and σ is the conductivity of the medium in S/m. Ohm's law relates **J** and **E**:

$$\mathbf{J} = \sigma \mathbf{E}. \tag{3}$$

To reduce the complexity of the computations, two-dimensional (2-D) blocks are used to represent the Earth. For a layered Earth, various blocks with different conductivities assumed to be uniform within each block are used to represent a section of the Earth which intersects the location of the Grassridge station. This has proven to be a very convenient assumption in GIC modeling and is adopted in this work. If the geomagnetic field is then assumed to be a plane wave propagating downward, the derived mathematical expressions are identical to the basic magnetotelluric equation derived by *Cagniard* [1953] for a uniform Earth as given in equation (4) which is also applicable in layered Earth.

$$E_{x,y}(\omega) = \pm \frac{Z}{\mu_0} B_{y,x}(\omega) \tag{4}$$

and

$$Z(\omega) = \sqrt{\frac{\omega}{\mu_0 \sigma}} exp^{\frac{i\pi}{4}}, \tag{5}$$

where $Z(\omega)$ is the surface impedance in Ω and ω is the angular frequency.

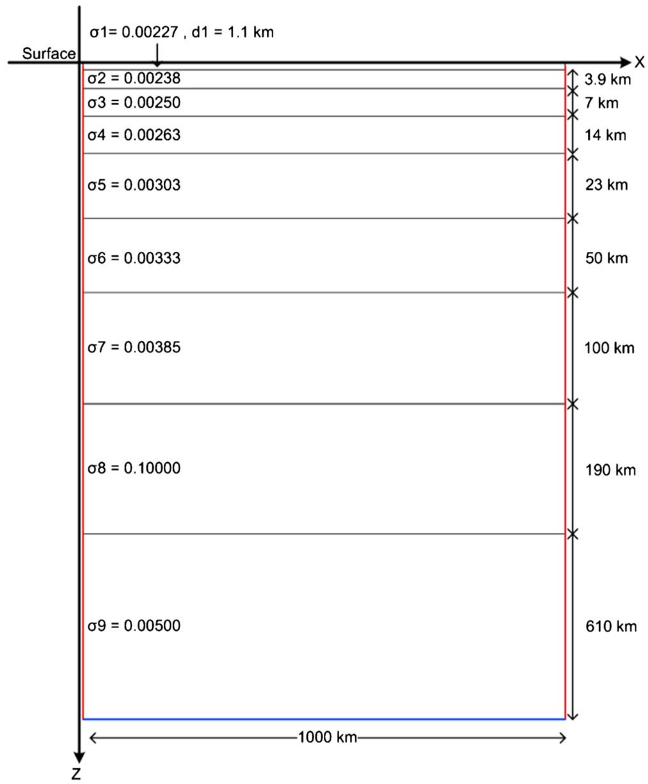

Figure 2. Layered Earth model as used in the 2-D FEM. Figure not drawn to scale. The 1000 km in the *x* direction was taken to make the lateral extent of the model much larger than the depth. For 2-D model, the blocks are assumed to be of infinite extent and uniform in the *y* direction.

3.2. GIC Computation

Once the geophysical step is executed, the computation of GIC is straightforward. In our case we compute GIC in the time domain as follows:

$$\mathrm{GIC}(t) = aE_x(t) + bE_y(t), \tag{6}$$

where *a* and *b* are the network coefficients which have units A km/V which can be expressed as conductivity time area. The coefficients are unique for the particular substation where the GIC are computed, in this case Grassridge. These coefficients map the geoelectric field fluctuations, through the physical configuration of the power grid, to the GIC.

4. Data Sources

The geomagnetic data selected were that of the first day of the Halloween storm that occurred from 29 October 2003 to 31 October 2003. The 1 min International Real-time Magnetic Observatory Network (INTERMAGNET) geomagnetic field data used as the model input were measured at HER (34.4°S, 19.24°E) and HBK (27.74°S, 25.94°E). Only the horizontal magnetic field components of the data were used (X = north and Y = east).

Measured GIC at GSS (33.74°S, 25.64°E) were used for comparison with modeled GIC. The GIC were measured in the neutral connection of the autotransformer connected to the 400 kV busbar.

5. Method

In the current work we used the COMSOL Multiphysics FEM modeling package for the computation of electric field for a layered Earth. COMSOL Multiphysics is considered to be a "general-purpose software platform, based on advanced numerical methods, for modeling and simulating physics-based problems" [*COMSOL Inc.* 2014]. The choice of this platform was motivated by the variety of physics it is designed to handle.

The layered Earth model is defined in the simulation platform in 2-D as shown in Figure 2. The conductivity profile used was derived by *Ngwira et al.* [2008] through the computation of the surface impedance using methods developed by *Pulkkinen et al.* [2007].

The *AC/DC* module, which allows computation of electric and magnetic fields over a wide frequency band, was used [*COMSOL Inc.* 2012]. The measured magnetic field data are applied to the surface of the Earth's model (surface indicated in Figure 2). The computations are done in the time domain using the COMSOL *time-dependent* study. The output of the computation is the induced electric field in the layers of the Earth due to the variations in the magnetic field data. The *magnetic field* option in COMSOL for solving the Maxwell's equations was chosen. For each modeled layer, equation (7) is solved and the induced electric field is expressed by equation (8).

$$\sigma \frac{\partial \mathbf{A}}{\partial t} + \nabla \times \left(\frac{\mathbf{B}}{\mu_0 \mu_r} \right) - \sigma \mathbf{v} \times \mathbf{B} = \mathbf{J_e} \tag{7}$$

and

$$\mathbf{E} = \frac{\mathbf{J_e}}{\sigma}, \tag{8}$$

where **A** is the magnetic potential vector, **B** is the applied magnetic flux density, σ is the conductivity, **v** is the velocity of the conductor (which is zero in the current case as there is no moving media in the model), μ_r is the relative permeability, and $\mathbf{J_e}$ is the current density.

To satisfy the requirement that the applied magnetic field remains constant within each layer, the "perfect magnetic conductor" boundary condition is applied to the left and right boundaries of the model. This boundary condition, implying $\mathbf{n} \times \mathbf{H} = 0$, prevents tangential components of the magnetic field at the edges of the model.

The network coefficients used in the computations are those derived by *Ngwira et al.* [2008] and the network coefficients we derive from the measured GIC and the computed electric field. We compare the results of the FEM model with those obtained by *Ngwira et al.* [2008] and by *Bernhardi et al.* [2008a] by computing the root-mean-square error (RMSE) based on equation (9), and the relative error (RE) based on equation (10) for the 24 h of 29 October 2003. Only the median RE for $|\mathrm{GIC}_{\mathrm{measured}}| > 1$ A is considered. The RMSE for the most active period of the storm, i.e., from 06:00 to 12:00 and 19:00 to 24:00 is also computed for comparison with the results by *Bernhardi et al.* [2008a] who focused on this part of the storm.

$$\mathrm{RMSE} = \sqrt{\frac{\sum_{i=1}^{n} (X_{\mathrm{obs},i} - X_{\mathrm{model},i})^2}{n}}, \tag{9}$$

where X_{obs} is the observed, X_{model} is the modeled GIC value measured at a time i, and n is the number of observations.

$$\mathrm{RE} = \frac{\mathrm{GIC}_{\mathrm{measured}} - \mathrm{GIC}_{\mathrm{modeled}}}{\mathrm{GIC}_{\mathrm{measured}}}. \tag{10}$$

We consider two cases for the geomagnetic input to the 2-D FEM model. The first case uses only the HER magnetic data (FEM1), while the second case uses the interpolated data from HER and HBK (FEM2).

6. Network Coefficient Estimation

The network coefficients are usually calculated using network analysis by taking into consideration the resistances and geometry of the power system. We propose another method which can be used to estimate the *a* and *b* coefficients from the time series of the horizontal geoelectric field components and the measured GIC. During a period where $E_x \simeq 0$, the corresponding GIC is mostly due to E_y. Equation (6) is therefore reduced to equation (11) during such periods.

$$\mathrm{GIC}(t_i) = bE_y(t_i), \tag{11}$$

$\forall_i$ where $E_x \simeq 0$ and t_i are the times of the selected observations.

A similar relation applies when $E_y \simeq 0$. The method is tested in this work using the FEM-computed geoelectric field. We derive the *a* and *b* coefficients from interpolated magnetic field data of 29 October 2003 using the following steps:

1. The horizontal electric field components E_x and E_y are computed.
2. The angle of the electric field E_x and E_y is determined.
3. The network coefficients are estimated for events meeting specific criteria that insured both the GIC and the geoelectric field, E, were well above noise level. For GIC the criteria were $|\mathrm{GIC}| > 0.1$*rms (GIC). Direction and magnitude criteria were imposed for E. Only events with electric field angles within of the north-south direction (*a* coefficient criteria) or within of the east-west directions (*b* coefficient criteria) were examined. Further restrictions on the electric field component magnitudes were the following: for coefficient *a*, $|E_x| > 0.7$*rms(E_x) and $|E_y| < 0.1$*rms(E_y) and for coefficient *b*, $|E_y 1| > 0.7$*rms(E_y) and $|E_x| < 0.1$*rms(E_x). An example of a set of the estimated coefficients that are selected for computation is illustrated in Figure 3. In total there were 31 instances when the *a* coefficient was estimated and 11 instances when the *b* coefficient was estimated.

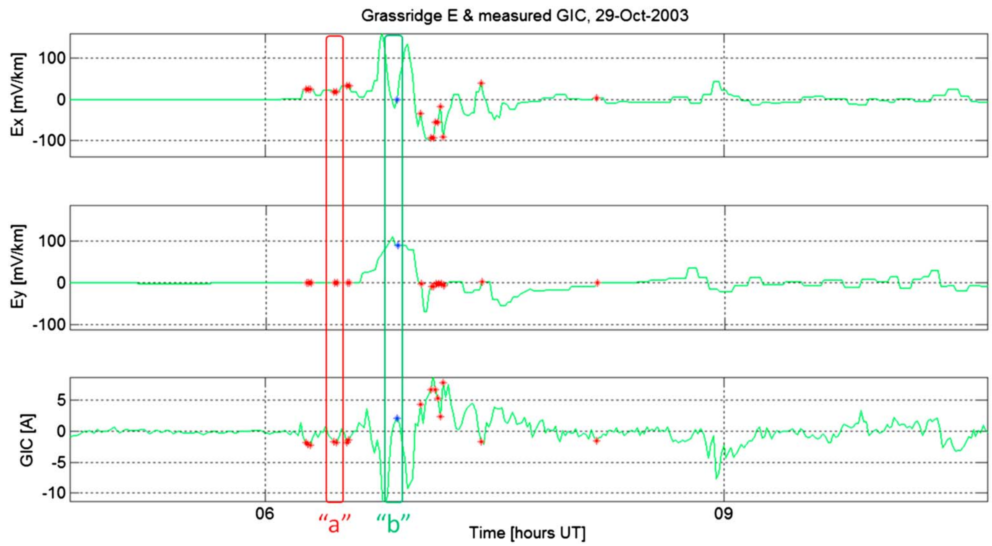

Figure 3. Typical events that were selected for the estimation of the *a* and *b* coefficients. The red stars mark events used for estimation of the *a* coefficient, and the blue stars mark events used for the estimation of the *b* coefficient.

4. The estimated coefficients from the previous step are evaluated for consistency and further processed as needed. Figure 4 shows the estimated coefficients for intervals meeting the criteria in step 3 during the geomagnetic storm of 29 October 2003. These estimates were arranged in the order of decreasing GIC. The polarity of the estimated *a* coefficient was consistently positive. For coefficient *a*, outlier values that significantly increased the standard deviations of the data set were discarded. The result was that first 10 values for *a* were averaged to give $a = -94$ A km/V as the network coefficient for the north-south geoelectric field response. Because the *b* coefficient polarity was inconsistent, *b* was estimated by fitting to the average value of the *a* coefficient to give the best match of the calculated GIC with the measured GIC. The result was $b = 24$ A km/V for the east-west geoelectric field response. The coefficients $a = -94$ A km/V and $b = 24$ A km/V are hereafter called the "new" network coefficients.

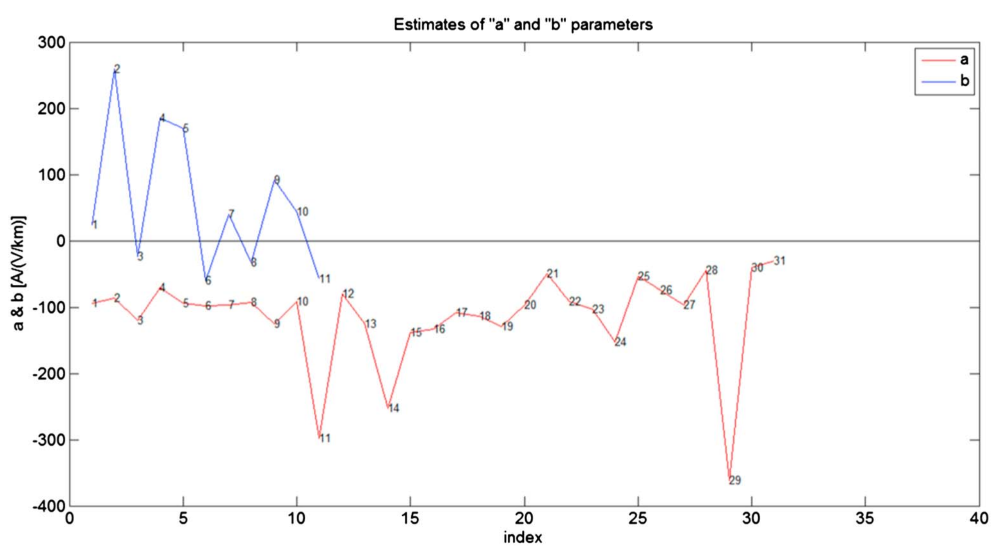

Figure 4. The estimates of the *a* and *b* coefficients using the proposed new method for a selected part of the storm of 29 October 2003. The estimated values are arranged in the order of decreasing GIC with index 1 corresponding to the event where |GIC| was largest.

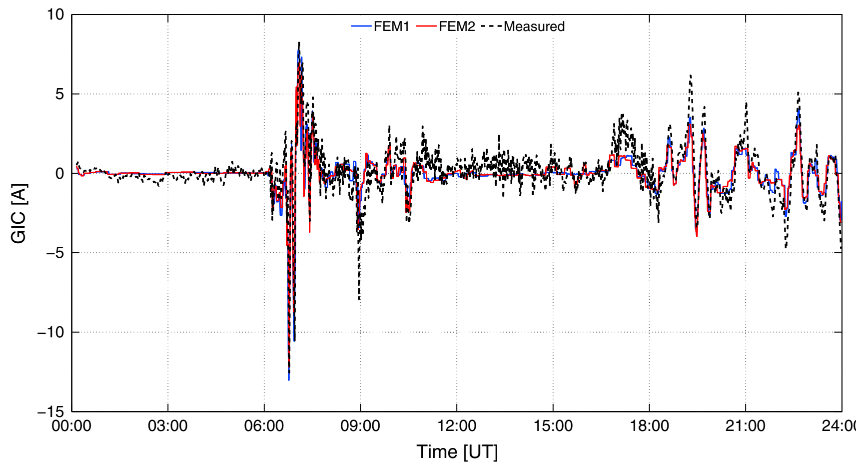

Figure 5. Comparison of modeled and measured GIC at Grassridge for 29 October 2003 using the Ngwira network coefficients $a = -80$ and $b = 1$ Akm/V. See Table 1 for details.

7. Results

The comparison of the modeled GIC with the measured GIC indicated that there is a correlation as illustrated in Figure 5. Figure 6 compares the modeled and measured GIC for the most active parts of the storm, i.e., the period 06:00–12:00 UT and 19:00–24:00 UT computed using the network coefficients $a = -80$ and $b = 1$ A km/V (henceforth referred to as "Ngwira" coefficients). Figures 7 and 8 show the results of using the new network coefficients. The RMSE, the RE, and the maximum currents for 29 October 2003 for both sets of network coefficients are presented in Table 1. Figures 9 and 10 show the error defined by $GIC_{measured} - GIC_{modeled}$ and the error distribution for 29 October 2003 with a bin width of 1 A for the Ngwira and new network coefficients, respectively. The two figures indicate that the use of the two different sets of network coefficients does not result in a significant change in the error distribution.

7.1. Results Assessment

The modeling was done in 2-D. The FEM computation time of the geoelectric field for 24 h of data sampled at 1 min is approximately 1 min on a Desktop PC (i5-3474 at 3.20 GHz, 8 Gb random-access memory, 64 bit) for each B field component, either B_x or B_y.

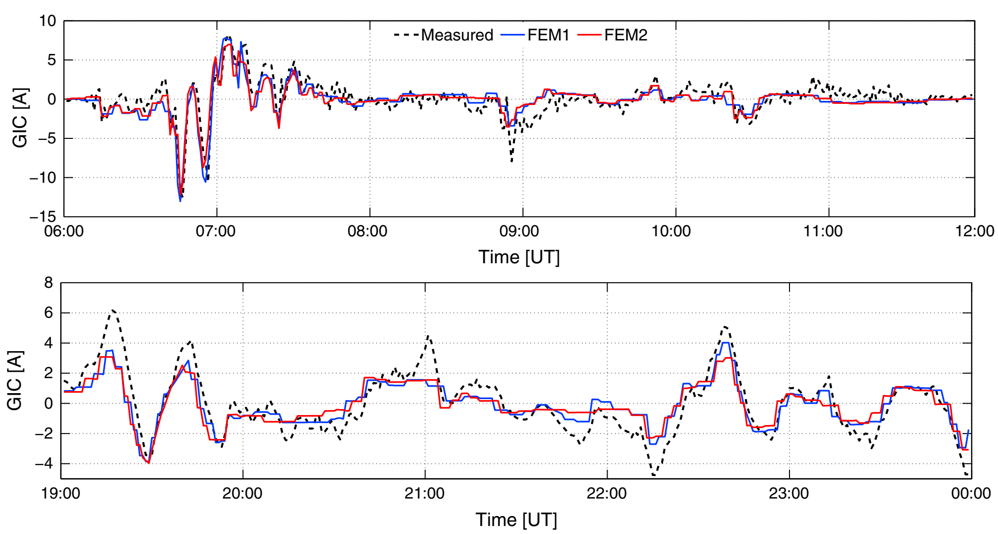

Figure 6. Comparison of modeled and measured GIC for the most active parts of the magnetic storm for the periods 06:00–12:00 UT and 19:00–24:00 UT on 29 October 2003 using Ngwira network coefficients $a = -80$ and $b = 1$ Akm/V.

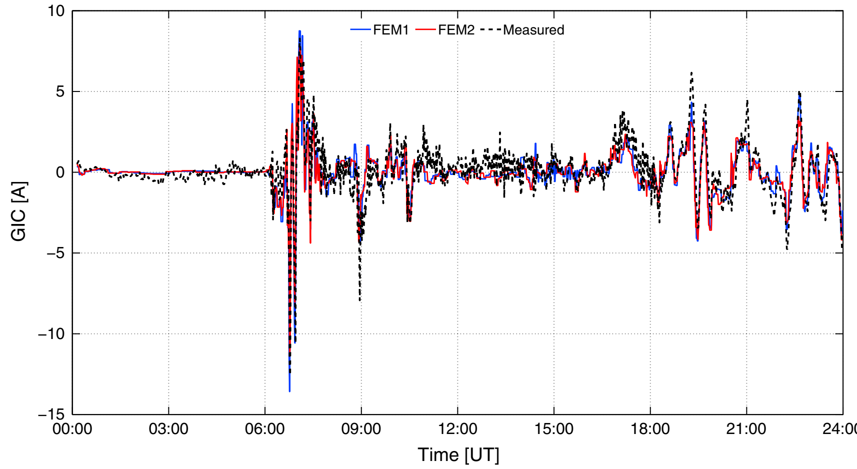

Figure 7. Comparison of the modeled and measured GIC using the new network coefficients, $a = -94$ and $b = 24$ Akm/V for the 24 h period on 29 October 2003.

As highlighted in *Ngwira et al.* [2008] and *Bernhardi et al.* [2008a], the important attribute of a good model is its ability to estimate the maximum current that is likely to occur at a particular substation during a storm. The most significant contribution to estimate the peak GIC comes from the *a* and *b* coefficients as they will affect the outcome of the computed GIC. From the work reported by *Ngwira et al.* [2008], RE of 48% and RMSE of 1.59 were obtained from their model where the magnetic field measured at HER was used. In the current work, for the same data (FEM1), a RE of 51% and RMSE of 1.35 are obtained. The interpolated data (FEM2) give a higher RE of 55% but a lower RMSE of 1.31 for the Ngwira network coefficients. Details of the maximum current estimated by the *Ngwira et al.* [2008] model are not given. In the present study the maximum difference between the modeled and measured values of GIC is 0.4 A for both sets of magnetic field data. The only difference is that FEM1 gave a peak value which was 0.4 A above the measured value while FEM2 underestimated the measured GIC by 0.4 A. The RMSE of the most active part of the storm period was the same for both cases of magnetic field. HBK-only data were not considered at all in the study based on the results reported by *Bernhardi et al.* [2008a] which indicated relatively high RMSE for a homogeneous Earth model with only HBK data.

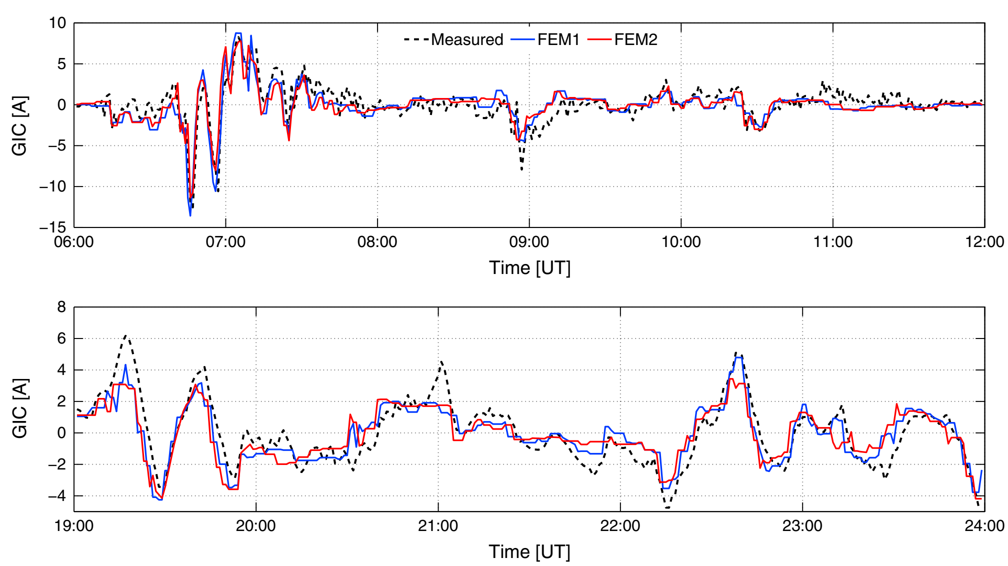

Figure 8. Comparison of modeled and measured GIC for the most active parts of the magnetic storm for the periods 06:00–12:00 UT and 19:00–24:00 UT on 29 October 2003 using the new network coefficients, $a = -94$ and $b = 24$ Akm/V.

Table 1. Comparison of the Maximum Estimated Current, RMSE for Two Periods, and the RE for the Measured and Modeled GIC for the Two Sets of Network Coefficients and Two Cases of the Magnetic Field

Data	Max I (A)	RMSE 06:00–12:00	RMSE 19:00–24:00	RMSE 00:00–24:00	RE 00:00–24:00 (%)
	$a = -80$, $b = 1$ A km/V			*(Ngwira Set)*	
Measured	12.6				
FEM1	13.0	0.96	1.07	1.35	51
FEM2	12.2	0.97	1.14	1.31	55
	$a = -94$, $b = 24$ A km/V			*(New Set)*	
Measured	12.6				
FEM1	13.6	1.38	1.11	0.98	41
FEM2	11.4	1.41	1.21	1.02	47

When the new *a* and *b* coefficients are used for the GIC computation, there are some notable changes in the modeled GIC. There is an average increase of 0.43 A in the RMSE for the most active part of the storm (06:00–12:00 h UT) compared to the GIC using the Ngwira coefficients. However, the 24 h RMSE is reduced by 0.37 A and 0.27 A for FEM1 and FEM2, respectively, by using the new coefficients. The RE is reduced by an average of 9% for both magnetic field cases. The maximum current estimation deviates from the measured by 1A for FEM1 (overestimation) and 1.2 A for FEM2 (underestimation).

Figures 6 and 8 demonstrates that during periods when $\partial B/\partial t$ is high, there is a good correlation between the measured and the modeled GIC. For instance, for the period 06:00–12:00 h the correlation coefficient is 81% (FEM1) and 79%(FEM2) when using the Ngwira coefficients and 82% for both FEM1 and FEM2 when using new coefficients. The correlation coefficient for the period 19:00–24:00 h is 86% for both FEM1 and FEM2 for the Ngwira coefficients and 89% (FEM1) and 87%, (FEM2) when the new coefficients are used. The correlation coefficients are not as good during periods of low $\partial B/\partial t$, e.g., 12:00–19:00 where they are 59% (FEM1), 57% (FEM2) for the Ngwira coefficients and 66% (FEM1) and 64% (FEM2) for the new coefficients.

The error distributions in Figures 8 and 9 are not significantly different, despite the difference between the Ngwira and the new values for the *a* and *b* coefficients. The ratio of *a*(new) to *a*(Ngwira) is about 1.17 while the ratio of *b*(new) to *b*(Ngwira) is 24. Thus, the GIC error distribution seems to be much less sensitive to the variation in the *b* parameter than in the *a* parameter. This is attributed to the fact that the power line terminating at the Grassridge station runs almost north-south which makes the GIC in this line insensitive

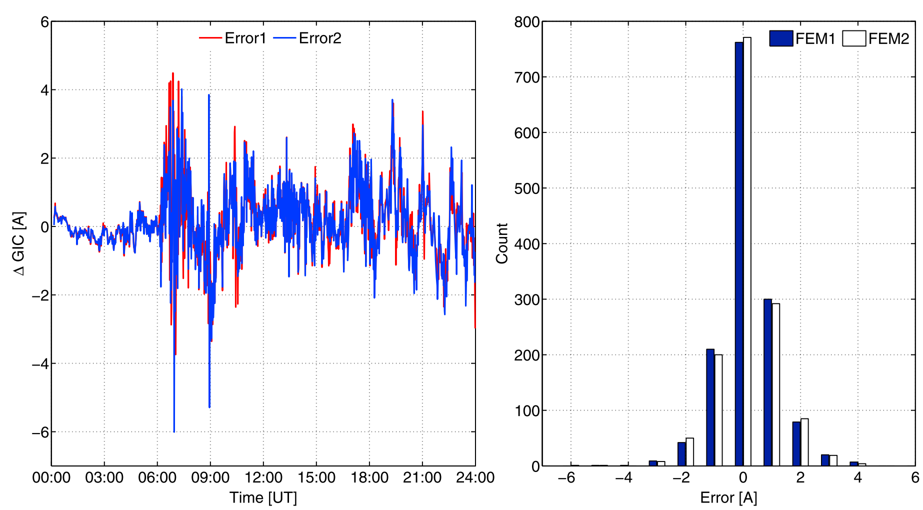

Figure 9. Error and error distribution derived from GIC modeled with the Ngwira coefficients, $a = -80$ and $b = 1$ A km/V for the 24 h period on 29 October 2003. Error1 = $GIC_{measured} - GIC_{FEM1}$ and Error2 = $GIC_{measured} - GIC_{FEM2}$.

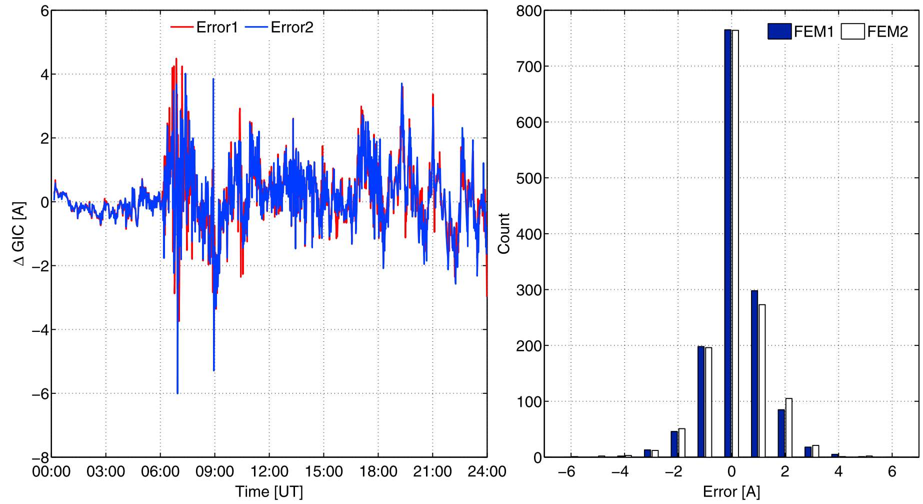

Figure 10. Error and error distribution derived from GIC modeled with the new coefficients, $a = -94$ and $b = 24$ A km/V for the 24 h period on 29 October 2003. Error1 = $\mathrm{GIC}_{\mathrm{measured}} - \mathrm{GIC}_{\mathrm{FEM1}}$ and Error2 = $\mathrm{GIC}_{\mathrm{measured}} - \mathrm{GIC}_{\mathrm{FEM2}}$.

to the E_y component of the field. The insensitivity of the GIC to the E_y component of the field is also confirmed by the relatively large variation in the estimates of *b* in Figure 4 compared to the variation in the estimates of *a*.

8. Conclusions

The study presented only focused on the 29 October 2003 (Halloween) storm which had a significant impact on the South African power grid. Some transformer failures were reported in different parts of the South African grid [*Gaunt and Coetzee*, 2007]. Using magnetic field data and GIC data recorded during this period can therefore be considered to be a significant step in modeling GIC in the South African power grid. Good quality GIC data were not available from Grassridge for any other geomagnetic storms.

The 2-D finite element model used for modeling the geoelectric fields demonstrated that the finite element method is an effective tool for geoelectric field computation in connection with GIC estimation as it is fast and the modeled GIC compare well with measured GIC. The use of the interpolated geomagnetic data from these two selected stations does not give a distinctive difference in the modeled GIC relative to use of data from HER only. This differs from the conclusions by *Bernhardi et al.* [2008a, 2008b]. In the current case, using only HER data gives slightly better results with the new network coefficients $a = -94$ A km/V and b = 24 A km/V.

The method proposed for calculating the network coefficient is very simple as it does not require the knowledge of the network configuration. GIC modeled with the new set of network coefficients have shown an improvement on the GIC model in terms of the correlation coefficient and the errors computed. These new approaches are an advance in modeling GIC in the South African power grid.

Acknowledgments
The data used for Figures 3–10 are available in the supporting information Table S1. The GIC data were obtained from the South African power utility, ESKOM. Interested persons could contact the authors for details of the current contact person at ESKOM. The results presented in this paper rely on the data collected at the HER and HBK observatories. We thank SANSA for supporting their operation and INTERMAGNET for promoting high standards of magnetic observatory practice (www.intermagnet.org). The research is supported by a grant from the South African National Space Agency (SANSA). We appreciate the contributions of David Oyedokun and Stefan Lotz of SANSA Space Science to the discussions on this paper.

References

Amm, O., and A. Viljanen (1999), Ionospheric disturbance magnetic field continuation from the ground to the ionosphere using spherical elementary current systems, *Earth Planets Space*, *51*, 341–440.

Bernhardi, E. H., T. A. Tjimbandi, P. J. Cilliers, and C. T. Gaunt (2008a), Improved calculation of geomagnetically induced currents in power networks in low-latitude regions, Power System Computation Conference, Scotland.

Bernhardi, E. H., P. J. Cilliers, and C. T. Gaunt (2008b), Improvement in the modelling of geomagnetically induced currents in Southern Africa, *S. Afr. J. Sci.*, *104*, 265–272.

Bolduc, L. (2002), GIC observations and studies in the Hydro-Quebec power system, *Astrophys. Sol. Terr. Phys.*, *64*(16), 1793–1802.

Boteler, D. H., and R. J. Pirjola (1998), The complex-image method for calculating the magnetic and electric fields produced at the surface of the Earth by the auroral electrojet, *Geophys. J. Int.*, *132*, 31–40.

Boteler, D. H., R. Pirjola, and H. Nevanlinna (1998), The effects of geomagnetic disturbances on electrical systems at the Earth's surface, *Adv. Space Res.*, *22*(1), 17–27.

Cagniard, L. (1953), Basic theory of the magnetotelluric method of geophysical prospecting, *Geophysics*, *18*, 605–635.

COMSOL Inc. (2012), Introduction to the AC/DC module. [Available at http://www.comsol.com.]

COMSOL Inc. (2014), Introduction to COMSOL Multiphysics. [Available at http://www.comsol.com/comsol-multiphysics.]

Dong, B., D. W. Danskin, R. J. Pirjola, D. H. Boteler, and Z. Z. Wang (2013), Evaluating the applicability of the finite element method for modelling of geoelectric fields, *Ann. Geophys.*, *31*, 1689–1698.

Gaunt, C. T., and G. Coetzee (2007), *Transformer Failures in Regions Incorrectly Considered to Have Low GIC Risk*, IEEE, Powertech Conference, Switzerland.

Kappenman, J. G. (2007), Geomagnetic disturbances and impacts upon power system operation, in *The Electric Power Engineering Handbook*, 2nd ed., edited by L. L. Grigsby, pp. 16.1–16.22, CRC Press/IEEE Press, London.

Koen, J. (2000), Geomagnetically induced currents and its presence in the Eskom transmission network, Master's thesis, Univ. of Cape Town, Cape Town, South Africa.

Koen, J. (2002), Geomagnetically induced currents in the Southern African transmission network, PhD thesis, Univ. of Cape Town, Cape Town, South Africa.

Moldwin, M. B. (2008), *An Introduction to Space Weather*, Cambridge Univ. Press, New York.

Molinski, T. S. (2002), Why utilities respect geomagnetically induced currents, *Astrophys. Sol. Terr. Phys.*, *64*(16), 1765–1778.

Ngwira, C. M., A. Pulkkinen, L.-A. McKinnell, and P. J. Cilliers (2008), Improved modeling of geomagnetically induced currents in the South African power network, *Space Weather*, *6*, S11004, doi:10.1029/2008SW000408.

Ngwira, C. M., L.-A. McKinnell, P. J. Cilliers, A. Viljanen, and R. Pirjola (2009), Limitation of the modeling of the geomagnetically induced currents in the South African power network, *Space Weather*, *7*, S10002, doi:10.1029/2009SW000478.

Paul, C. R. (2004), *Electromagnetics for Engineers: With Applications to Digital Systems and Electromagnetic Interference*, John Wiley.

Pirjola, R. (2002), Review on the calculation of the surface electric and magnetic fields and of geomagnetically induced currents in ground based technologies, *Surv. Geophys.*, *23*, 71–90.

Pulkkinen, A. (2003), Geomagnetic induction during highly disturbed space weather conditions: Studies of ground effects, PhD thesis, Univ. of Helsinki, Helsinki, Finland.

Pulkkinen, A., R. Pirjola, and A. Viljanen (2007), Determination of the ground conductivity and system parameters for optimal modeling of geomagnetically induced current flow in technological systems, *Earth Planets Space*, *59*, 999–1006.

Shepherd, G. S., and F. Shubitidze (2003), Method of auxiliary sources for calculating the magnetic and electric fields induced in a layered Earth, *J. Atmos. Sol. Terr. Phys.*, *65*, 1151–1160.

Wik, M., A. Viljanen, R. Pirjola, A. Pulkkinen, P. Wintoft, and H. Lundstedt (2008), Calculation of geomagnetically induced currents in the 400 kV power grid in Southern Sweden, *Space Weather*, *6*, S07005, doi:10.1029/2007SW000343.